Longitudinal, transverse, and single-particle dynamics in liquid Zn: *Ab initio* study and theoretical analysis

B. G. del Rio and L. E. González
Departamento de Física Teórica, Universidad de Valladolid, 47011 Valladolid, Spain
(Received 8 March 2017; revised manuscript received 8 May 2017; published 1 June 2017)

We perform *ab initio* molecular dynamics simulations of liquid Zn near the melting point in order to study the longitudinal and transverse dynamic properties of the system. We find two propagating excitations in both of them in a wide range of wave vectors. This is in agreement with some experimental observations of the dynamic structure factor in the region around half the position of the main peak. Moreover, the two-mode structure in the transverse and longitudinal current correlation functions had also been previously observed in high pressure liquid metallic systems. We perform a theoretical analysis in order to investigate the possible origin of such two components by resorting to mode-coupling theories. They are found to describe qualitatively the appearance of two modes in the dynamics, but their relative intensities are not quantitatively reproduced. We suggest some possible improvements of the theory through the analysis of the structure of the memory functions. We also analyze the single-particle dynamics embedded in the velocity autocorrelation function, and explain its characteristics through mode-coupling concepts.

DOI: 10.1103/PhysRevB.95.224201

I. INTRODUCTION

The dynamic behavior of a liquid at long times (compared to interatomic collision times) and large length scales (compared to atomic sizes) can be well understood in terms of continuum theories, namely hydrodynamics. This indicates that only two mechanisms are required to understand longitudinal dynamics: thermal relaxation and adiabatic propagation of attenuated pressure waves (sound). Transverse stress can however only be relaxed via shear viscosity, since the lack of elasticity prevents the propagation of shear waves. In this hydrodynamic regime the dynamic structure factor of the liquid, $S(q,\omega)$, has the form of a Rayleigh-Brillouin triplet, with a central Lorentzian peak, whose width is related to the thermal diffusivity, and a pair of stretched-Lorentzian side peaks at positive and negative frequencies, whose position is dictated by the adiabatic sound velocity and whose width is related to the sound attenuation. The transverse spectrum is also Lorentzian, and its width is related to the shear viscosity [1,2].

This picture changes when the explored length scales and times decrease, entering in the so-called kinetic regime. Additional mechanisms can appear in the longitudinal dynamics (for instance, structural relaxation), leading to a more complex behavior, and viscoelasticity of the liquid can lead to the emergence of shear waves for wave vectors larger than a critical one [1,2].

If length scales become smaller than interatomic distances and times shorter than collision times, the dynamics are dictated by free-particle-like motion (lacking therefore any type of collective wave propagation), which is characterized simply by the thermal velocity of the particles. In this regime the correlation functions take a Gaussian form [1,2].

The kinetic regime is by far the one less well understood, and this has prompted experimental as well as theoretical studies of liquid dynamics in this regime, which comprises wave vectors q spanning typically the range from 10^{-1} to 10^{1} Å^{-1} and frequencies ω in the THz range. Experimental techniques include inelastic scattering of radiation, either x rays or neutrons, which exchange energy and momentum with the density fluctuations in the liquid. These studies only probe longitudinal dynamics, and have shown that, in general, the shape of the dynamic structure factor evolves from the Rayleigh-Brillouin hydrodynamic form by changing the positions of the peak frequencies, reflecting the dispersion of the collective longitudinal excitations, and varying the widths of the central and side peaks. This type of behavior has been reproduced by molecular dynamics simulation studies, and also by different theoretical approaches. Transverse dynamics is, on the other hand, not accessible directly to experimental techniques for liquids, and their study relies on molecular dynamics simulations and/or theoretical approaches. The general behavior obtained through these methods is, as mentioned before, the transition from pure relaxation at small q values, to a propagating scenario above a critical q. Upon increasing the wave vector (decreasing the length scale explored) the dynamics eventually become free-particle-like and propagation again disappears.

Recently, however, a careful analysis of the measured scattering intensities in several liquid metals has unveiled the existence of a second propagating excitation in a wave-vector region around $q_p/2$, where q_p is the position of the main peak of the static structure factor, $S(q)$, of the liquid [3–11]. Interestingly, the frequency associated to this excitation is similar to the one associated to transverse waves at the same wave vector. This fact prompted the interpretation of this second contribution as a fingerprint of transverse excitations in the longitudinal spectrum. Such interpretation is merely based on the similarity of the corresponding frequencies, but it is not backed by any theoretical approach that may explain such coupling between transverse and longitudinal excitations.

A similar situation appears in relation with the transverse dynamics. Recent studies of high-pressure liquid Li, Fe, and Na have unveiled the existence of two (not just one) propagating excitations in the transverse dynamics [12], now for wave vectors around q_p. In this case a tentative interpretation would be to attribute the second mode to the coupling with longitudinal propagating excitations. Moreover, analysis of the

longitudinal currents in this region also suggest the existence of two propagating modes. It was first assumed that this type of behavior was a pressure-induced effect, but more recent calculations for liquid Ni at room pressure have unveiled a quite similar behavior [11]. Again, the association of these phenomena to coupling between longitudinal and transverse modes has not been backed by theoretical schemes yet.

In this paper we try to make some advance into the explanation of such couplings as responsible for the two-mode structure of the longitudinal and transverse spectra, using in particular mode-coupling ideas. Mode-coupling theories were developed starting in the 1970s and, since then, they have been mostly applied in simplified forms to the study of the dynamic glass transition [13]. There have been some applications to the study of the longitudinal dynamics of a few liquid metals but none for the transverse dynamics yet. The basic idea of mode-coupling approaches is to separate the dynamics into two contributions with different decay rates. A fast one is related mostly to binary collisions, although it can also include couplings with fast-decaying modes. A second, slowly decaying, contribution is due to the coupling of the magnitude studied with hydrodynamic modes, which vary slowly for small wave vectors. This decomposition is performed at the level of the memory functions, as introduced by Mori and Zwanzig [2,14].

Our study is here applied to the dynamics of liquid Zn (l-Zn). This system is among those for which a second mode in $S(q,\omega)$ around $q_p/2$ has been suggested by experimental observation. In fact it has been found both in inelastic x-ray scattering (IXS) experiments [6] and in inelastic neutron-scattering (INS) experiments [7]. Zinc has a full d shell that contributes in an essential way to its properties. The structure of Zn systems is quite peculiar in all phases, from clusters [15] to the hcp solid phase, where a very large c/a ratio is observed [16], to the liquid, where an asymmetric main peak is found [17–19]. Most of these characteristics are shared only with Cd, which is immediately below in the periodic table. Such complexities obviously demand the use of highly accurate methods to describe the interatomic interactions.

We have determined the dynamic properties of liquid Zn (l-Zn) through molecular dynamics (MD) simulations, where the total energy and the forces on the atoms are evaluated *ab initio* on the fly using density functional theory (DFT) [20]. This type of simulation, referred to as *ab initio* molecular dynamics (AIMD), is very accurate, but also very costly computationally, and therefore the simulated samples are relatively small. We have, however, performed rather long simulation runs in order to keep the statistical noise as small as feasible.

Single-particle dynamics can also be computed from molecular dynamics runs, and we will show the results for the velocity autocorrelation function (VACF) and its Fourier transform, usually called the power spectrum. The motion of a particle in a dense fluid is influenced by the motion of the "cage" of neighbors that surround it, against which it bounces, and therefore it can be easily understood that the behavior of collective magnitudes has some effect on the single-particle dynamics. This influence can be described in a way similar to that considered previously for the collective dynamics, i.e., the memory function of the VACF can be separated into fast and slow components, with the latter determined by the coupling with slow modes [21,22]. We have found it more convenient to follow a different route that includes the coupling of the particle velocity with longitudinal and transverse currents directly in the VACF [23]. This type of theory has already been applied to several liquids and yielded a good description of the VACF [10,24], so we check if it still holds in the complex dynamics scenario of l-Zn.

The layout of the paper is as follows: in Sec. II we describe briefly the AIMD simulation setup, in Sec. III we define the magnitudes studied and the theoretical approaches used, in Sec. IV we show the results obtained for collective dynamics from both the simulation (Sec. IV A) and the theoretical approach (Sec. IV B). The last section is devoted to the analysis of the velocity autocorrelation function obtained through the simulation and from the theoretical approach. Some conclusions are finally drawn, and possible improvements in the theoretical analysis are discussed. The Appendix goes through the full mathematical expressions used in the theoretical study.

II. COMPUTATIONAL DETAILS

We have enclosed 90 Zn atoms into a cubic simulation cell of side $L = 11.35$ Å, so that the ionic number density is $\rho = 0.061\,55$ atoms/Å^3. We have considered explicitly 12 valence electrons per atom ($10d + 2s$), and their interaction with ionic cores has been modeled through an ultrasoft pseudopotential taken from the dataset included within the VASP utility [25]. This code has been used in order to perform the molecular dynamics run, evaluating for each configuration the ground-state energy from DFT and the forces on the atoms through the Helmann-Feynmann theorem. The exchange and correlation energy has been treated within the generalized gradient approximation using the Perdew-Burke-Ernzerhof (PBE) parametrization and nonlinear core corrections have also been included. The cutoff for the plane-wave expansion of the orbitals has been 300 eV. The ionic equations of motion have been solved using a time step of 4 fs.

After the equilibration period, when the temperature has stabilized at 723 K, we have let the system evolve for 36 000 configurations (144 ps), and these configurations have been used in order to sample the properties of interest which were subsequently analyzed as described below.

The atomic positions and velocities at each time step are directly available from the simulations, so that any function depending on them can be computed straightforwardly. Moreover, the periodic boundary conditions associated to the simulation box fix the wave vectors compatible with the imposed periodicity, and consequently $\vec{q}$-dependent magnitudes can only be obtained for such a set of wave vectors. In particular the minimum feasible wave vector is $q_{\min} = 2\pi/L = 0.55$ Å^{-1}.

III. THEORY

A basic variable used in the description of the dynamic properties of a monoatomic liquid is the $\vec{q}$-dependent particle density, defined as $\rho(\vec{q},t) = \sum_i \exp[-i\vec{q}\cdot\vec{r}_i]$, where i runs over particles and $\vec{r}_i$ denote their positions.

The liquid static structure factor $S(q)$ is obtained as the autocorrelation of this magnitude at equal times (averaged over

wave vectors with the same module and over configurations), whereas the intermediate scattering function $F(q,t)$ is its time autocorrelation function (now averaged over wave vectors and time origins),

$$F(q,t) = \frac{1}{N}\langle \rho(\vec{q},t+t_0)\rho(-\vec{q},t_0)\rangle. \quad (1)$$

The dynamic structure factor $S(q,\omega)$ is the Fourier transform (FT) of $F(q,t)$ into the frequency domain. The scattered intensity in an IXS experiment for given momentum and energy transfer (after the background signal has been substracted), $I(q,E)$, is directly related to $S(q,\omega)$, if appropriate corrections for detailed balance and energy resolution are applied. In the case of INS experiments the signal also includes incoherent contributions that must be accounted for, but in the particular case of Zn the incoherent cross section is very small, so it can be considered a purely coherent scatterer. For INS measurements additional contributions corresponding to multiple scattering are in general also important and must be appropriately substracted.

Another most important dynamic magnitude is the $\vec{q}$-dependent particle current, defined as $\vec{j}(\vec{q},t) = \sum_i \vec{v}_i \exp[-i\vec{q}\cdot\vec{r}_i]$, with $\vec{v}_i$ the particle's velocity. The $\vec{j}$ vector is then decomposed into a term parallel to $\vec{q}$, which is the longitudinal current, and a term perpendicular to $\vec{q}$, which is the transverse current. Obviously the longitudinal current can be described by a number, but the transverse current is a vector. The corresponding time autocorrelation functions are

$$C_L(q,t) = \frac{1}{N}\langle j_L(\vec{q},t+t_0)j_L(-\vec{q},t_0)\rangle, \quad (2)$$

and

$$C_T(q,t) = \frac{1}{2N}\langle \vec{j}_T(\vec{q},t+t_0)\cdot\vec{j}_T(-\vec{q},t_0)\rangle. \quad (3)$$

Note that, by definition, $C_L(q,t) = -\ddot{F}(q,t)/q^2$, where the dot denotes the time derivative, and consequently, $C_L(q,\omega) = \omega^2 S(q,\omega)/q^2$, so both functions reflect exactly the same information.

Rotational symmetry in the system implies that these two polarizations are independent and do not mix directly, and that the correlation function between any two coordinate components of the current vector is uniquely determined by C_L and C_T. The instantaneous configuration of atoms in a liquid is not spherically symmetric (even more so in simulations where a periodicity of the simulation cell is imposed) so that some transverse-longitudinal mixing might occur, but such direct mixing should be expected to be quite small. The existence of transient structures (such as "dimers") that destroy rotational symmetry has been suggested to justify the mixing, but the argument is not totally convincing, since the lifetime of such structures is very short, and, moreover, not all liquids exhibit them.

We propose below a different approach, where the coupling between longitudinal and transverse modes does not occur directly, at the same wave vector, but indirectly, through all possible wave vectors, using mode-coupling ideas. These are routinely posed in terms of memory functions of the autocorrelation functions, which are described next.

A. Memory functions

The memory function of the intermediate scattering function can be defined either in the time domain or in the Laplace transform (LT) domain:

$$\dot{F}(t) = -\int_0^t d\tau M(\tau)F(|t-\tau|)\,;\ \tilde{F}(z) = \frac{F_0}{z+\tilde{M}(z)}, \quad (4)$$

where $F_0 = F(t=0)$, is the initial value of the function, and the tilde denotes the LT, $\tilde{F}(z) = \int_0^\infty dt F(t)\exp[-zt]$.

The same procedure can be followed for any time-dependent function, so we also define $N(q,t)$ as the memory function of $M(q,t)$, i.e., the second-order memory function of $F(q,t)$, and $M_T(q,t)$ as the memory function of $C_T(q,t)$.

Note that the short-time behavior of the correlation functions and the memory functions (also related to their frequency moments) is dictated by static properties which can be directly evaluated from atomic positions, velocities, accelerations, and, if necessary, higher-order derivatives of the positions. Also note that the odd-order initial time derivatives of the correlation functions and memory functions must vanish due to time-reversal symmetry.

An interesting feature of memory functions is that usually their time decay is faster than that of the original function. Therefore at some point in the memory function hierarchy it is possible to invoke a Markovian approximation, according to which the decay of a certain order memory function is instantaneous, thus leading to a simplified model for the previous lower-order memory function, namely an exponential function,

$$f_{\mathrm{Ex}}(t) = a\exp[-bt], \quad \tilde{f}_{\mathrm{Ex}}(z) = \frac{a}{z+b}. \quad (5)$$

The particular form of the LT of an exponential function (a rational function of z of first degree in the denominator) means that all the previous lower-order memory functions are also rational functions of z (of higher degrees in the denominator). These can then be separated into simple fractions, leading therefore to a sum of several exponential functions in the time domain. The number of exponential functions increases by 1 for each level one moves up in the hierarchy of memory functions. In the next subsection we mention several models of this type, frequently used in the analysis of MD or experimental data. We note however that exponential functions do not behave correctly for short times, since the odd-order derivatives are different from zero. Consequently we also propose some modified models that behave as exponentials for long times but whose odd-order initial time derivatives vanish.

B. Models

The hydrodynamic model for $F(q,t)$ and $C_T(q,t)$ can be cast as models for $N(q,t)$ and $M_T(q,t)$ respectively [26]. On one hand $N(q,t)$ is modeled by the sum of a Dirac-δ function due to an instantaneous viscous relaxation and an exponential function due to a slower thermal relaxation. This leads to an $M(q,t)$ with two exponentials and finally an $F(q,t)$ with three exponential functions. On the other hand $M_T(q,t)$ is modeled by a Dirac-δ function due to instantaneous shear relaxation, leading to an exponential $C_T(q,t)$.

Since all the coefficients in the LT of the memory functions are real numbers, the roots of the denominator must appear either as real numbers or as complex conjugate (c.c.) pairs, and the same happens to the corresponding amplitudes in the partial fraction decomposition. A pair of c.c. exponentials is in fact a damped oscillatory function of time. The three exponentials in $F(q,t)$ in the hydrodynamic model turn out to be a real one and a pair of c.c. ones, which represent respectively relaxing and propagating contributions to the longitudinal dynamics, as mentioned in the Introduction. In $S(q,\omega)$ the real root leads to the central line of the Rayleigh-Brillouin triplet, while the pair of c.c. roots leads to the positive and negative frequency side peaks.

The immediate generalization of the hydrodynamic model consists of substituting the instantaneous relaxations by exponential ones, so that $N(q,t)$ is then the sum of two exponentials [three for $M(q,t)$ and four for $F(q,t)$, respectively], whereas $M_T(q,t)$ is modeled by one exponential, and consequently $C_T(q,t)$ by the sum of two exponential functions. Out of the four exponentials in $F(q,t)$ two turn out to be a c.c. pair, and the other two real ones. Consequently, there are two central Lorentzian lines and the positive and negative frequency side peaks in $S(q,\omega)$. Such a model is usually named as either a generalized hydrodynamic model or a viscoelastic model, depending on the physical interpretation for the fast and slow components of $N(q,t)$. Regarding the transverse dynamics it turns out that for small q the two roots are real, while for wave vectors larger than some critical q they become a c.c. pair, so that propagation of shear waves sets in. This model for the transverse dynamics is again usually named as viscoelastic model.

Further models can be easily constructed by including more exponentials. For instance, if one wants to describe two different propagating modes and a relaxation mode in $F(q,t)$, as suggested by the appearance of fingerprints of transverse modes in the measured or computed $S(q,\omega)$ near $q \approx q_p/2$, then at least five exponentials are needed in $F(q,t)$ (a real one and two pairs of c.c. roots), which means that $N(q,t)$ must be represented by at least three exponentials. These three could either be all real or be one real and one c.c. pair. Note that in the second case $N(q,t)$ should show an oscillatory behavior. Similarly, if one wants to have two propagating modes in $C_T(q,t)$ as observed around $q \approx q_p$ for several systems, then at least two c.c. pairs are needed, leading to an $M_T(q,t)$ with at least three exponential functions, which again may be all real or else a real one and an oscillatory term due to a c.c. pair. Therefore we may say that the presence of an oscillatory component in the memory functions $N(q,t)$ or $M_T(q,t)$ hints towards the possible existence of two propagating modes in the longitudinal or transverse dynamics respectively.

The particular properties of the LT of exponential functions justifies their use in models, but it is important not to forget that these functions do not behave analytically as correlation functions or memory function should, namely they do not have null odd order derivatives at $t = 0$. Obviously a combination of such functions can be forced to fulfill these (or at least some of these) requirements. One particular case of such a combination is the so-called damped harmonic oscillator (DHO) model, widely used in the interpretation of experimentally measured IXS and INS spectra to represent propagating excitations. This amounts to a pair of c.c. exponentials with particular coefficients that nullify the first derivative at $t = 0$, namely,

$$f_{\mathrm{DHO}}(t) = a \exp[-\gamma t]\left(\cos(\omega_o t) + \frac{\gamma}{\omega_o}\sin(\omega_o t)\right). \quad (6)$$

While the first derivative behaves correctly, one runs into problems for higher-order derivatives. For instance, the $C_L(q,t)$ function corresponding to such a mode in $F(q,t)$ would contain a term of the form $-\ddot{f}_{\mathrm{DHO}}(t)$, and it is easy to verify that such a function violates the condition of initial null derivative [the third derivative of $f_{\mathrm{DHO}}(t)$ at $t = 0$ is nonzero].

While forcing the correct derivatives is possible when including a sufficient number of exponentials [27], using such an approach it may be complicated to disentangle if the presence of a particular exponential function is due to a physical process that decays/oscillates with that particular rate/frequency, or is just due to the mathematical requirement of nullifying the odd derivatives at short times. It therefore seems useful to introduce some modifications into these model functions so as to guarantee the correct time behavior, while still maintaining the long-time behavior of the exponential functions. We propose here the following models to replace the exponential and DHO ones:

$$f_{\mathrm{mEx}}(t) = \frac{a}{\cosh(bt)}, \quad (7)$$

$$f_{\mathrm{mDHO}}(t) = c\left(\frac{\cos(\omega_o t)}{\cosh(\gamma t)} + \frac{\gamma}{\omega_o}\frac{\sin(\omega_o t)}{\sinh(\gamma t)}\right). \quad (8)$$

These types of models will be used later in order to check the q range where two propagating modes can be found and to analyze the structure of the memory functions obtained from our simulations.

C. Mode-coupling theories

When studying the behavior of the correlation function or the memory functions of a given dynamic variable, it is often found that they exhibit several rates of decay. Only the slowest one survives for long times, and the main idea behind mode-coupling (MC) theories, is that this long-lasting term comes from the coupling of the variable studied with other slowly decaying ones (modes). The development of MC theories started in the 1970s and they have been derived to study the correlation function of several magnitudes, such as a particle velocity (velocity autocorrelation function) [28], the single-particle density (self-intermediate scattering function) [29], the particle density (intermediate scattering function) [30], and the transverse current (transverse current correlation function) [28]. The slowly decaying modes included in the different theories include the single-particle density, the particle density, its time derivative, the longitudinal current, and the transverse current.

A very successful application of MC ideas has been the study of structural arrest in undercooled liquids, which signals a variant of glass formation (see, for a review, Ref. [13]). Basically one seeks for the possibility that $F(q_p,t)$ develops a solution that does not decay to zero for long times. MC theories have also been applied to dense gases, high-temperature liquids or hard-sphere models, where, for

instance, they explain the appearance of an algebraic decay in the velocity autocorrelation function.

Their application to liquids near their melting temperature is however somewhat more scarce; for a recent review see Ref. [31]. In order to study this type of system, the original MC theories were modified during the 1980s so as to consider not only the long-time behavior but also the short-time one [2,21,22,32]. This part is mostly caused by binary atomic collisions, but it can also include couplings with fast decaying modes. Basically a heuristic treatment of this part is performed, rewriting the MC part in a way that it vanishes rapidly (as t^4) for short times, and modeling the fast part by a Gaussian-like function that incorporates the full value and initial decay of the memory function being considered. Such modifications were spurred by the observations of Levesque and Verlet about the memory function of $Z(t)$ obtained by MD simulations for LJ systems [33]. These modified theories have been applied at different levels of approximation and self-consistency by several groups to study the dynamic properties of LJ systems, liquid alkalis, liquid Pb, and liquid Sn and liquid Ge [21,22,34–40].

We have applied the MC formalism to study the longitudinal dynamics, where the fast/slow decomposition is performed at the level of $N(q,t)$, and the transverse dynamics, where the decomposition is performed at the level of $M_T(q,t)$, namely,

$$N(q,t) = N^f(q,t) + N^{\mathrm{MC}}(q,t), \tag{9}$$

$$M_T(q,t) = M_T^f(q,t) + M_T^{\mathrm{MC}}(q,t). \tag{10}$$

In the mode-coupling components we include only the particle density as a slow mode, so that these terms appear as integrals over wave vectors of functions that involve the intermediate scattering functions. The full expressions for the fast and MC components are given in the Appendix, and more details can be found in Ref. [2].

D. Velocity autocorrelation function

The VACF is defined as the normalized autocorrelation function of a particle's velocity, i.e.,

$$Z(t) = \langle \vec{v}(t+t_0)\cdot\vec{v}(t_0)\rangle / \langle \vec{v}(t_0)\cdot\vec{v}(t_0)\rangle, \tag{11}$$

where the average is over particles and time origins. It describes how, on average, a particle loses memory of its initial value and direction, due to collisions with other particles. The typical shape of $Z(t)$ in a dense liquid shows a negative minimum, due to velocity reversal after a collision with a particle that belongs to the "cage" of nearest neighbors that surrounds it. Then a damped oscillatory behavior follows towards zero for long times. Its time integral is related to the diffusion coefficient, and its initial second derivative is related to the so-called Einstein frequency that describes an average oscillation frequency within the neighboring cage [2].

There are several theories that try to quantify the influence of slowly decaying collective variables on the behavior of $Z(t)$. For instance, Wahnström and Sjögren [22] put forward a MC theory in the same spirit as that mentioned above for collective currents, namely, the memory function of $Z(t)$ is split into a fast term and a MC term given in terms of an integral over wave vectors. A different approach was followed by Gaskell and Miller [23], who considered a "velocity field" of the fluid, and analyzed how this is influenced by longitudinal and transverse currents using mode-coupling ideas. This led to an integral formula for $Z(t)$ (not its memory function), that incorporates longitudinal and transverse current correlation functions:

$$Z_{\mathrm{GM}}(t) = \frac{1}{24\pi^3}\int d\vec{q}\; f(q)F_s(q,t)[C_L(q,t) + 2C_T(q,t)]. \tag{12}$$

Here $f(q)$ is the FT of a normalized function that describes a particle's localization, usually taken as the Wigner-Seitz sphere. In this case the expression is $f(q) = (3/\rho)j_1(aq)/(aq)$, where $(4/3)\pi a^3 = 1/\rho$, and $j_1(x)$ is the spherical Bessel function of the first order.

Separating the sum in the integral into its two parts, each defines naturally the longitudinal $Z^L_{\mathrm{GM}}(t)$ and transverse $Z^T_{\mathrm{GM}}(t)$ contributions to the VACF, coming from the couplings of the single-particle velocity with each of the polarizations of the collective current.

IV. COLLECTIVE DYNAMICS

A. AIMD simulation results

As a previous validation of the input parameters of the simulation, we have compared the static structure factor obtained from the simulations with the available experimental ones [17–19] (which agree well among themselves) as shown in Fig. 1. We find an excellent description of $S(q)$, including the asymmetric shape of the main peak, located at $q_p \approx 3.0$ Å^{-1}, and the amplitude and phase of the subsequent oscillations. The pair-correlation function $g(r)$ also compares favorably with the corresponding experimental data [17,19].

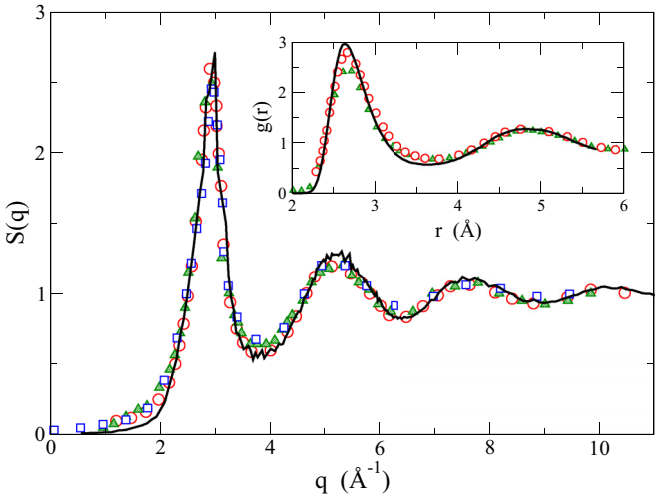

FIG. 1. $S(q)$ for l-Zn near melting. Full lines: simulation results. The symbols denote experimental measurements. Triangles: x-ray data from Ref. [17]; circles: x-ray data from Ref. [19]; squares: neutron data from Ref. [18]. The inset shows $g(r)$ with the same meaning for lines and symbols.

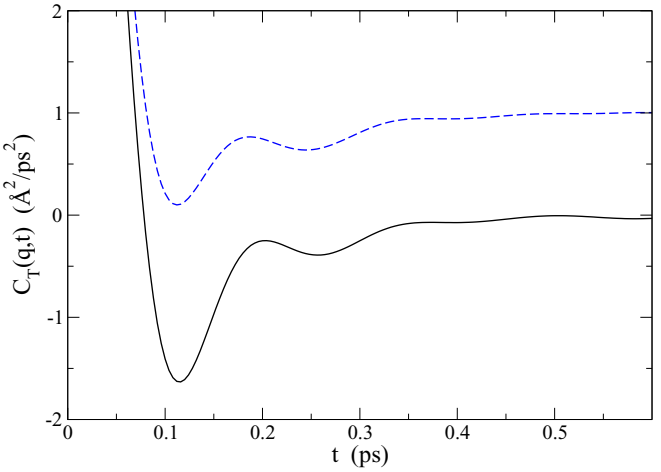

FIG. 2. Detail of $C_T(q,t)$ for $q = 1.84$ (full line) and 3.71 Å^{-1} (dashed line). The latter has been shifted up by one unit.

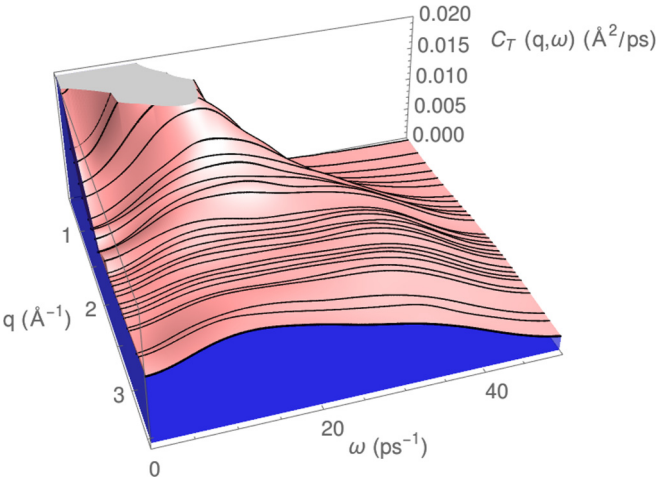

FIG. 3. Transverse current spectra, $C_T(q,\omega)$, in a wide q range.

1. *Transverse dynamics*

Traditionally, the behavior of transverse dynamics in liquids has been studied in the small-q region, where a transition between relaxation and propagation has been observed for many liquids. Only in recent years has some attention been paid to the behavior of transverse dynamics at higher q values, but still not as high as required to reach the free-particle regime. Surprisingly double peak structures in $C_T(q,\omega)$ have been found for liquid metals under pressure for wave vectors around q_p [9,10,12]. Liquid Ni at room pressure has been also found to exhibit a similar picture [11]. Based on these premises, we have undergone a detailed study of the transverse current correlation functions and corresponding spectra for l-Zn in an extended q range.

The lowest q value allowed by the simulation setup is already outside the hydrodynamic region, since $C_T(q,t)$ already displays a negative minimum (and the spectrum shows a peak) indicating that propagation of shear waves already takes place at this q. An interesting phenomenon that we have observed is the presence of a negative tail in the $C_T(q,t)$ functions. An example is shown for $q = 1.84$ and 3.71 Å^{-1} in Fig. 2 where it is clearly visible due to the small amplitude of the oscillations, but we have found it in the whole q range studied.

In Fig. 3 we display a general view of the behavior of $C_T(q,\omega)$ for $q_{\min} \leqslant q \leqslant 5$ Å^{-1}. Here, and in the rest of the paper, the "simulation" frequency-dependent functions shown in the figures have been obtained by numerical FT of the time-dependent functions which were obtained directly from the simulations, and not through the FT of a fit to such functions. In some figures we will indeed compare both routes, which have always led to very similar results. The numerical FT only required the use of a window function to alleviate the statistical noise present for long times. Figure 3 shows a transition between a single mode and two modes that occurs around 1.7 Å^{-1}, somewhat above $q_p/2$. Around q_p the shape is very flat, but for higher q the two-mode structure is clearly visible again. The results for several q below and above q_p are displayed in Fig. 4 for increased clarity. We have made a fit of $C_T(q,t)$ using one mDHO for the high-frequency component, and the sum of a mDHO and a negative mEx (due to the negative tail) for the rest. The results of this decomposition are also shown in Fig. 4 for $q = 2.54$ and 3.37 Å^{-1}. The results of the fit reveal also the appearance of the second, high-frequency, mode around 1.7 Å^{-1} (for smaller q the amplitude of the high-frequency term found in the fit is negligible).

We can therefore conclude that l-Zn, as well as Ni, presents this double mode structure in the transverse dynamics in a wide range of wave vectors starting somewhat above $q_p/2$, even at normal pressures.

2. *Longitudinal dynamics*

The double mode structure of $C_T(q,\omega)$ was also observed in $C_L(q,\omega)$ in the case of liquid Fe and Na under pressure [9,10]. We therefore analyze here the properties of this magnitude for l-Zn also in the same extended q range considered for the transverse counterpart. It is however important to perform this study taking into account at the same time the dynamic

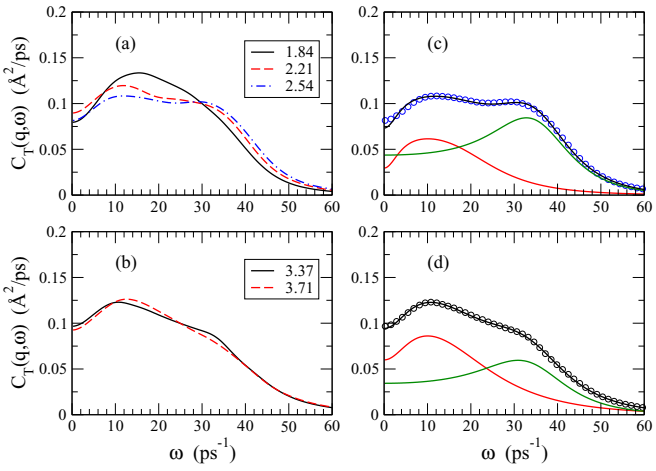

FIG. 4. $C_T(q,\omega)$ for wave vectors shown in the graphs. (a) Below q_p. (b) Above q_p. (c) Results for $q = 2.54$ Å^{-1}; circles: simulation data; lines: fit results and its two components. (d) Same as (c), but for $q = 3.37$ Å^{-1}.

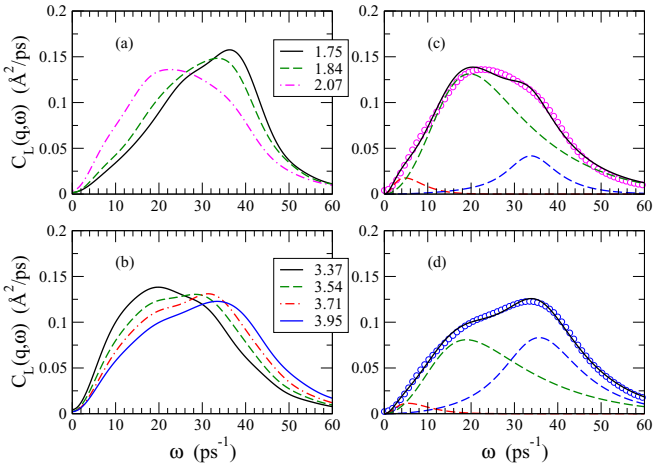

FIG. 5. $C_L(q,\omega)$ for wave vectors shown in the graphs. (a) Below q_p. (b) Above q_p. (c) Results for $q = 2.07$ Å^{-1}; circles: simulation data; lines: fit results and its three components. (d) Same as (c), but for $q = 3.95$ Å^{-1}.

structure factor $S(q,\omega)$, first because being directly related they should be described by the same terms if any decomposition into different contributions is performed: if a mEx or mDHO term is present in $F(q,t)$, its second derivative must be present in $C_L(q,t)$, and second because of the possible presence of peaks in $C_L(q,\omega)$ unrelated to propagating excitations. This is due to the fact that for small ω the function increases (starting at least as ω^2 according to its definition) and for large ω it decays to zero [as dictated by the null initial time derivative of $C_L(q,t)$], so that somewhere in between a maximum must exist, irrespective the presence or absence of propagating excitations. This property is however specific to $C_L(q,\omega)$ and, consequently, the comparison with $S(q,\omega)$ can be useful to discriminate the origin of the peak. For instance, in the free particle regime, for large q, $S(q,\omega)$ has a monotonic Gaussian form of width related to the thermal velocity, but $C_L(q,\omega)$ has a peak at a frequency related to this thermal velocity, totally unrelated to propagating collective excitations.

The separation into different contributions common to both $F(q,t)$ and $C_L(q,t)$ can be complicated for some wave vectors because of the different amplitudes of the corresponding terms in the two functions. For instance in the region around q_p a relaxing term is overwhelmingly dominant in $F(q,t)$ because of the structural correlations that lead to the de Gennes narrowing of $S(q,\omega)$. However such a term alone describes poorly the longitudinal current correlation function, and propagating terms are indeed needed, even if their contribution to $F(q,t)$ is insignificant. So when we consider below the components coming from a separation into contributions it must be understood that we have fitted jointly $F(q,t)$ and $C_L(q,t)$ to a given common model and using obviously the same parameters. We note in this respect the convenience of using models that fulfill directly the zero initial derivative of both $F(q,t)$ and $C_L(q,t)$ (as the mEx and mDHO ones) so as to obtain the correct short-time behavior of both functions.

In Fig. 5 we plot the AIMD calculated $C_L(q,\omega)$ for several wave vectors below and above q_p. The behavior observed is rather similar to the one found in the transverse case. A

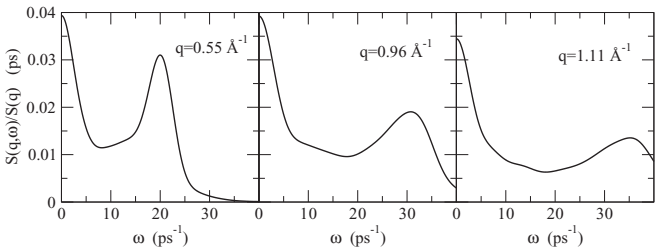

FIG. 6. $S(q,\omega)$ for some q values in the 1psBZ.

two-mode character of the functions is clearly observed. When approaching q_p from below the high-frequency component hardly changes its position, but its amplitude decreases strongly. On the contrary, the amplitude of the low-frequency component increases, while its position decreases. The switch from the high- to the low-frequency dominance in amplitudes produces a sharp decrease in the frequency corresponding to the maximum of $C_L(q,\omega)$ for q between 1.84 and 2.07 Å^{-1}. For wave vectors above q_p the opposite trend is found, with the amplitude of the low-frequency mode decreasing with q in favor of the high-frequency component, and a steep change in the position of the maximum from low to high frequencies. The decomposition of $C_L(q,\omega)$ into contributions is shown for two q values in the right panels of Fig. 5. Two mDHOs and one mEx were used in the common fits of $F(q,t)$ and $C_L(q,t)$ and it is interesting to observe the contribution of the relaxing mEx mode at small ω, which introduces a kind of bump in C_L at low frequencies.

Note that the analysis performed above includes the region of wave vectors larger that $q_p/2$, where the two-mode structure of the transverse and longitudinal currents is more visible. However, experimental measurements of $S(q,\omega)$ were performed in the q range below $q_p/2$, usually called first pseudo-Brillouin zone (1psBZ), and it is in this region where the measurements have suggested the existence of two propagating modes, with a low-frequency one that produces a small signal in the measured intensity at an energy located roughly between the quasielastic line and the usual intense inelastic one.

Figure 6 shows the results obtained from our simulations, for a few q values in this range. We clearly observe an unusual shape of $S(q,\omega)$ between the quasielastic and inelastic lines, which is qualitatively consistent with the IXS and INS results [6,7]. A more detailed comparison with experiments requires the conversion from the calculated $S(q,\omega)$ to the equivalent measured $I(q,E)$, which comprises the application of the detailed balance correction, convolution with experimental resolution function, and scaling (to arbitrary units as given in experiments). We show such comparison in Fig. 7, where we see a general overall agreement between the IXS experiment [6] and simulation, except for the height of the quasielastic line. However, the specific interline region shows indeed a similar shape, which was attributed in the experimental study to fingerprints of the influence of transverse excitations into the longitudinal dynamics. This was due to the good fitting of the experimental data obtained using a central Lorentzian line and two DHOs, suggesting the existence of two propagating excitations [6]. The INS experiments led to

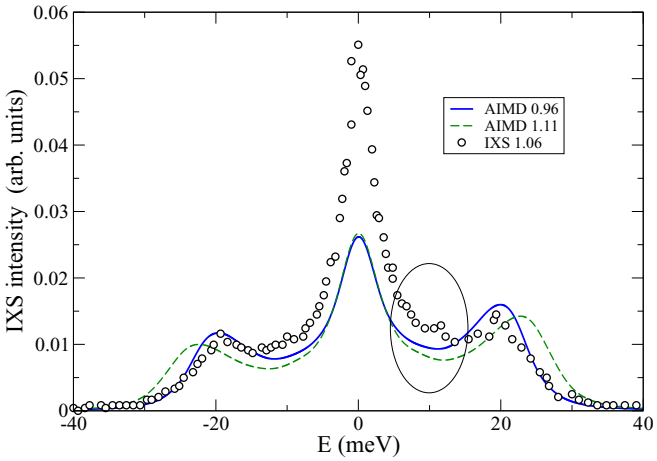

FIG. 7. Comparison of IXS measurements at $q = 1.06$ Å^{-1} and AIMD $I(q,E)$ obtained from the properly modified $S(q,\omega)$ (see text) for $q = 0.96$ and 1.11 Å^{-1}.

a similar conclusion, although the model used in fitting the $I(q,E)$ was different [7].

We show in Fig. 8 the AIMD results for the three functions $S(q,\omega)$, $C_L(q,\omega)$, and $C_T(q,\omega)$, scaled so as to fit in the same graph, in order to attest (i) the coincidence of the "features" in $S(q,\omega)$ with those of the longitudinal current spectra, which also display an "odd" shape in the corresponding frequency region, and (ii) the proximity between the frequencies of these features and the single maximum of C_T. Both q values shown are within the 1psBZ.

The global situation is summarized in Fig. 9, where we plot in several ways the results of the fits of the AIMD data to sums of one mEx and two mDHO models to all the functions considered, as discussed previously. For each mDHO we obtain an oscillation frequency ω_o and a damping rate γ. We define the natural oscillator frequency (that is, the one if there were no damping) as $\Omega_+ = \sqrt{\omega_o^2 + \gamma^2}$. This value is very close to the position of the maximum of the product of ω^2 and the FT of the mDHO. We also define the apparent frequency as $\Omega_- = \sqrt{\omega_o^2 - \gamma^2}$, which is very close to the position of the maximum of the FT of the mDHO (assuming that $\gamma < \omega_o$, otherwise the maximum occurs at $\omega = 0$). Therefore, if the

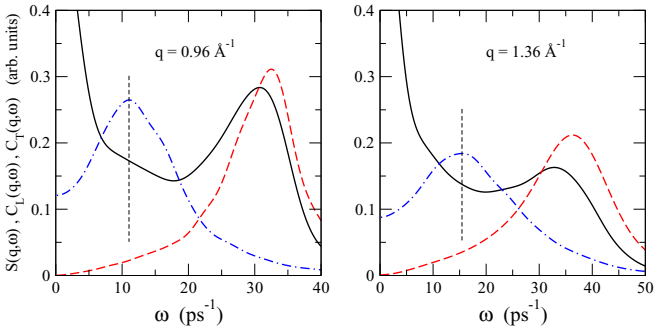

FIG. 8. Comparison among $S(q,\omega)$ (full line), $C_L(q,\omega)$ (dashed line), and $C_T(q,\omega)$ (dash-dotted line), scaled so as to fit in the same graph, for two q values in the 1psBZ. The vertical lines denote the position of the maximum of $C_T(q,\omega)$.

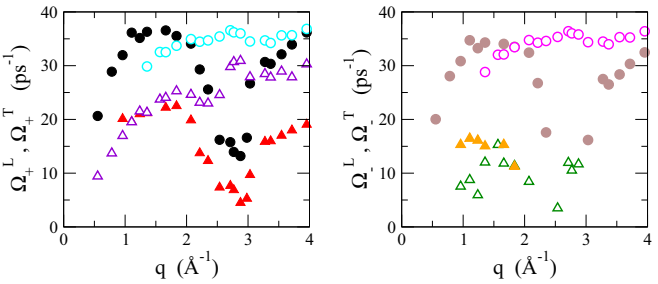

FIG. 9. Left panel: longitudinal and transverse natural frequencies. Circles: high-energy modes. Triangles: low-energy modes. Full symbols: longitudinal modes. Open symbols: transverse modes. Right panel: corresponding apparent frequencies. Symbols have the same meaning as in the left panel.

mDHO would be the only mode present one should see a maximum in $S(q,\omega \approx \Omega_-^L)$ and in $C_L(q,\omega \approx \Omega_+^L)$ for the $\Omega_\pm^L$ obtained in the common fit to these functions. Similarly one should find a maximum in $C_T(q,\omega \approx \Omega_-^T)$ for the Ω_-^T found in the fit. Note that no special feature would be seen at the natural transverse frequency Ω_+^T. In fact, the existence of other modes, with varying frequencies, damping coefficients, and amplitudes, can result in changing somewhat the position of the maxima, turning the individual peaks into shoulders or even masking them completely if the amplitudes are small.

We have plotted in Fig. 9 the natural frequencies in the left panel and the apparent frequencies in the right panel, for both the longitudinal and the transverse dynamics. We see that up to a wave vector around 1.2 Å^{-1} the transverse dynamics is well described with just one mDHO, but for larger q a two-mode model describes better the AIMD data. In the case of the longitudinal dynamics the crossover from one to two modes happens around 0.9 Å^{-1}. Moreover, between 0.9 and 1.8 Å^{-1}, there is a coincidence between the low-energy longitudinal natural frequency and either the unique or the low-energy transverse natural frequency. On the other hand, the apparent mode frequencies have similar, but not so much coincident, values especially below 1.2 Å^{-1}, due to the different dampings of the longitudinal and transverse modes. It is remarkable that the high-frequency transverse modes, after they appear, disperse very little, and both their natural and their apparent frequencies stay rather close to the largest frequency of the high-energy longitudinal mode, which occurs around $q_p/2$.

B. Mode-coupling analysis

From the AIMD calculated $F(q,t)$ and $C_T(q,t)$ we have evaluated the corresponding AIMD memory functions, $N(q,t)$ and $M_T(q,t)$, solving the integrodifferential equations that define them [Eq. (4)].

We have also used the expressions provided in the Appendix in order to compute the fast and MC components. The initial values and curvatures of the fast terms are equal to those of the full functions, which have been obtained from the simulation $N(q,t)$ and $M_T(q,t)$ by fitting the short time region with a form $a_0 - a_2 t^2 + a_4 t^4$. The integrals that define the MC component involve the whole wave-vector range from zero to infinity. Obviously we have evaluated them only in the range in which we have computed the $F(q,t)$ functions, which goes from

$q_{\min}$ up to a maximum vector $q_{\max} \approx 2q_p$. Moreover, since the set of wave vectors is established by the periodic boundary conditions, the functions are obtained in an uneven grid of q values. The integrals have therefore been performed using the trapezoidal rule, which is convenient for such a type of grid. All these limitations have an influence on the accuracy of the computed MC integrals [41], but we do not expect a qualitative change in the form of the results as a consequence of these limitations. We instead consider that the accuracy of the whole theory has a much greater influence on the goodness of the results. For instance, the inclusion of additional slow modes or a more fundamental treatment of the fast components that appear in the theory could lead to more marked, even qualitative changes. We will consider this point below, after the presentation of the results.

We finally point out that we have evaluated $S(q,\omega)$ and $C_L(q,\omega)$ from the sine and cosine Fourier transforms of $N(q,t)$, and $C_T(q,\omega)$ from those of $M_T(q,t)$, through the memory function equations in the Laplace domain and the relation between Fourier and Laplace transformations. The explicit formulas are detailed in the Appendix.

1. Transverse dynamics

The results obtained through the MC formalism for $C_T(q,\omega)$ are compared with the AIMD ones in Fig. 10, for $q =$ 0.96, 2.35, and 3.28 Å^{-1}. The first wave vector corresponds to the region where only one mode appears, whereas the other two lie below and above q_p in the two-mode region. We observe a qualitative agreement between MC and AIMD results, in particular regarding the one- or two-mode feature. This means that the present MC formalism captures the main mechanisms responsible for the double mode structure, so that indeed the coupling with density fluctuations gives rise to such features. However, as mentioned above, the coupling is indirect, with all possible wave vectors, and not just the specific $\vec{q}$ being considered, and occurs at the level of the memory function through an integration over wave numbers k and p. The weight for the coupling with different wave vectors is dictated by the function $\gamma(q,k,p)$ defined in the Appendix. It is interesting to analyze how this function depends on its parameters (k,p). The function γ factorizes into a product of a structural term, $[S(k) - S(p)]^2/[S(k)S(p)]$ and a "geometric" factor that depends only on the magnitude of the wave vectors. The form of the structural term favors (k,p) regions where the structure factor has a small magnitude, and values of k and p that lead to large differences between $S(k)$ and $S(p)$. This term therefore is largest for $k \to 0$ and p around q_p, with further, but lower, maxima at the positions of the subsequent peaks of the structure factor (and interchanging k and p since the function is symmetric). Note that the structural term is zero for $k = p$. The geometric term, on the other hand, is zero at the limits of the integration region (a strip around the diagonal, see the Appendix) and is maximum at $k = p$. The general structure of the weighting function will therefore be dictated by the compromise between the differing behavior of each term, leading to maxima, in general, for "small" k and near $p \approx q_p$, assuming such values of k are within the integration region (which approximately means that q is between $q_p/2$ and the first minimum of $S(q)$, located around 3.75 Å^{-1}, which we will refer to as the intermediate q region). We show a glimpse of the weighting function $\gamma(q,k,p)$ in Fig. 11 for q values below $q_p/2$, around $q_p/2$, around q_p, and for a q value beyond the first minimum of $S(q)$. It can be observed that the structure of the weight function changes little in the intermediate q region, but is qualitatively different outside. Remarkably, the clipping due to the geometric factor leads to maxima of the weight function that occur in the vicinity of $k = q_p/2, p = q_p$ for wave vectors in the intermediate q region. Therefore the structure of $M_T^{\mathrm{MC}}(q,t)$ is basically the same in such region and consequently this can explain the lack of dispersion of the modes in $C_T(q,\omega)$ as observed in the AIMD simulations.

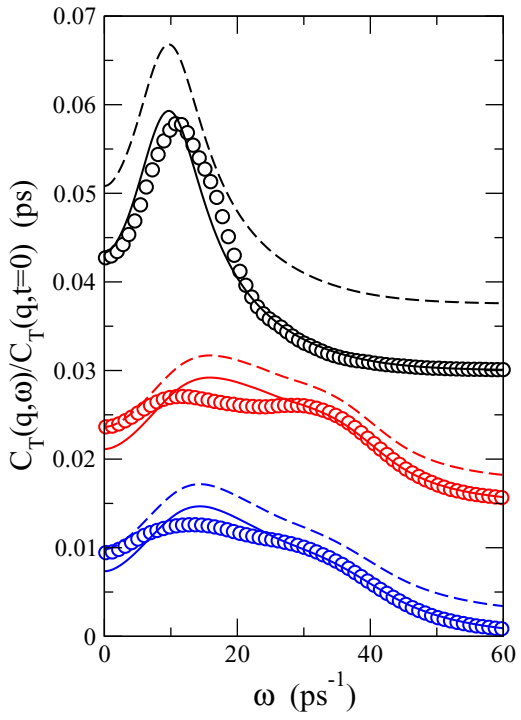

FIG. 10. Comparison between AIMD calculated $C_T(q,\omega)$, shown by symbols, and MC results, shown as lines. The q values shown are 0.96 Å^{-1} (displaced 0.03 units upwards), 2.35 Å^{-1} (displaced 0.015 units upwards), and 3.28 Å^{-1}. The lines are repeated slightly displaced above (dashed lines) in order to observe more clearly the double mode structure where it exists.

Although the presence of two modes is correctly described, the amplitude of the main, low-energy, one seems to be overestimated by the theory. In order to track down the origin of this problem we have compared directly the AIMD and MC memory functions, as shown in Fig. 12. The general shape, including the positions of maxima and minima when present, is reproduced. However, we find two weak points in the theory. The first is that the tail amplitude is in some cases overestimated, reflecting possibly the need to include additional slow variables in the MC contribution. The second problem is due to the fact that the mode-coupling component is always found to be positive, and the fast term, by construction, is also positive. Consequently the theory cannot reproduce the AIMD data whenever they show a negative minimum, which also coincides with the q region where the amplitude problem in $C_T(q,\omega)$ appears. A similar failure of the MC formalism to

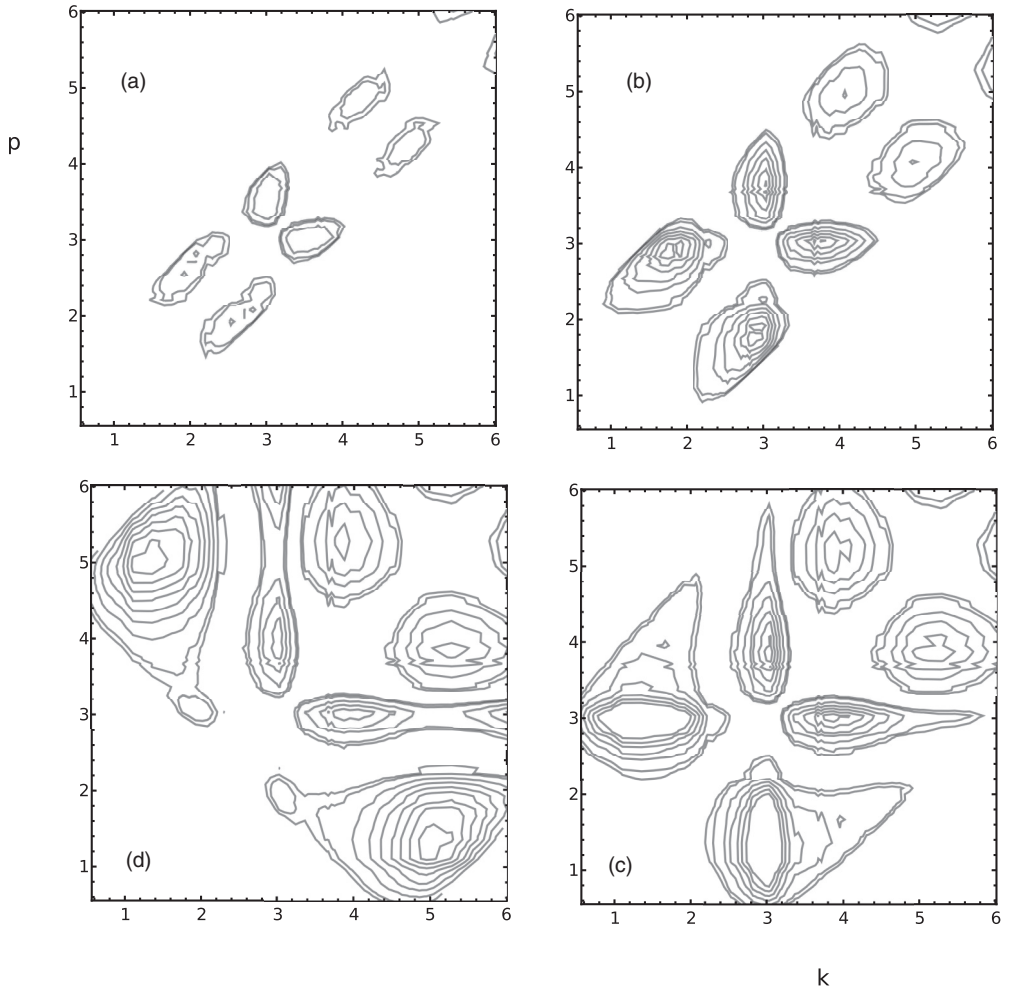

FIG. 11. Isolines for the weighting function $\gamma(q,k,p)$ at $q = 0.96$ (a), 1.57 (b), 2.98 (c), and 4.63 (d) Å^{-1}. The plotted contours correspond to 35 (closest to the diagonal), 50, 100, 150, . . . , units.

represent negative values in molecular dynamics data has been observed for the velocity autocorrelation function in liquid Pb [36], and in liquid Sn and Ge near the melting point and liquid Na at high temperatures [37].

We believe that the way towards the solution of these problems lies in a better treatment of the fast part of the memory function. As mentioned above, it includes not only the effects of binary collisions, but also the coupling with fast-decaying modes not included in the MC integral. These could indeed give rise to a negative minimum that would be reflected in an improved agreement with AIMD data. We therefore suggest the modification of the theory through the use of *Ansätze* for the fast term, different from the one used here, that incorporate a negative minimum in order to check the impact these would have in the quantitative description of the two-mode structure of $C_T(q,\omega)$. In fact, already in the seminal work of Levesque and Verlet on LJ systems [33] the second-order memory function of the intermediate scattering function was modeled using a fast term that has a negative minimum. Moreover, the *Ansatz* propsed by Wahnström and Sjögren for this same function [22] also becomes negative, as shown explicitly by Canales and Padró in their studies of liquid Li and LJ systems [39]. Even though we are considering here a different correlation function it seems plausible that a similar *Ansatz* may be useful.

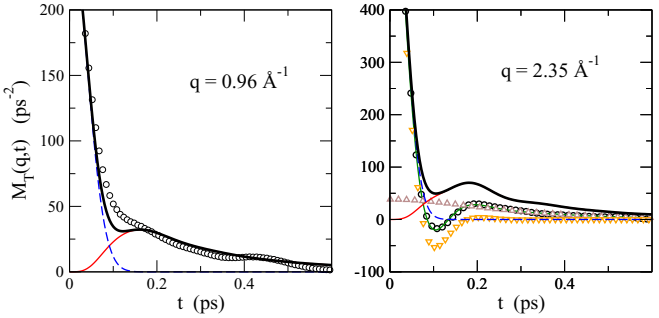

FIG. 12. $M_T(q,t)$ for the wavevectors shown. Circles: AIMD results. Dashed line: fast part. Thin red solid line: MC component. Thick solid line: total theoretical function. The thin green line is the fit of the AIMD results to the sum of a mEx slow term (up triangles) and a fast oscillating mDHO term (down triangles).

In connection with this point, we have tried to fit $M_T(q,t)$ with the models mentioned in the text above, and found that indeed one mEx and one mDHO describe well the AIMD data in the two-mode region. Curiously, as observed in Fig. 12 for $q = 2.35$ Å^{-1}, the mDHO turns out to be the fast term (which oscillates and takes negative values) while the mEx

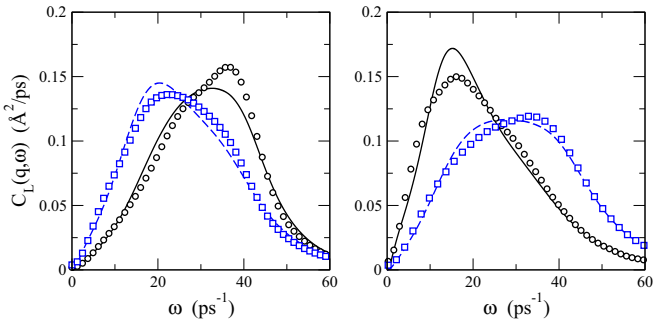

FIG. 13. Comparison between AIMD calculated $C_L(q,\omega)$, shown by symbols, and MC results, shown as lines. The q values shown are 1.75 Å^{-1} (full line and circles) and 2.07 Å^{-1} (dashed line and squares) in the left panel, and 3.27 Å^{-1} (full line and circles) and 4.07 Å^{-1} (dashed line and squares) in the right panel.

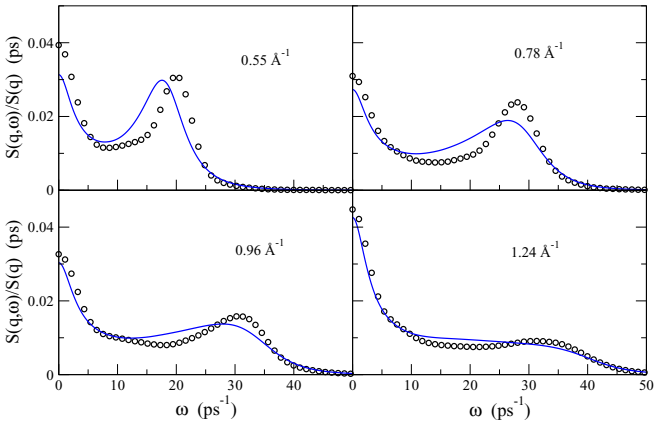

FIG. 14. Comparison between AIMD calculated $S(q,\omega)$, shown by symbols, and MC results, shown as lines. The q values are shown in the graphs.

term decays slowly, but does not go to zero for small times. We expect this information can also be useful in considering possible modifications to the MC theory in order to improve its accuracy.

In this context, as a final note, we also mention a diagrammatic formulation of the kinetic theory of fluctuations in equilibrium classical fluids, developed by Andersen and collaborators, who studied in particular the short-time behavior of the memory functions (akin to the fast term discussed here) [42]. The calculation of this short-time part for a LJ liquid within such an approach [43] indeed produced terms with a fast decay, but they do not account for the total value of the memory function at $t = 0$.

2. *Longitudinal dynamics*

We show in Fig. 13 $C_L(q,\omega)$ as obtained through the MC formalism, compared with the AIMD results in the q range where the double mode feature is visible in the simulations. Clearly, the theory describes correctly the mechanisms behind the appearance of this two-mode structure, including their frequencies and also the variation of the amplitudes with q, as evinced by the shifts in the main peak position in small intervals of q below (left panel) and above q_p (right panel), that was described previously.

The dynamic structure factor obtained from the AIMD simulations also showed traits of two propagating modes for some q values in the 1psBZ. The corresponding MC results are compared with the AIMD ones in Fig. 14. Here the theory basically misses the second propagating mode, and even the usual sound mode appears at too low a frequency in the MC data at the smallest q allowed by the simulation setup, although this can be due to the absence of coupling with temperature fluctuations in the theory, which is important for small q. Only for $q \approx 0.96$ Å^{-1} does the theory start showing some hints of an additional mode in the expected frequency region, but there is still much room for improvement in this important wave vector region. Taking into account that only the density has been considered as a slow mode to couple with, it seems natural to conclude that further modes need to be included in the MC formalism, out of which the most obvious one would be the transverse current mode. Such a possibility will be explored elsewhere and reported in due course.

One could also consider the possible existence of a problem with the fast component of $N(q,t)$ similar to the one found in $M_T(q,t)$, namely the presence of negative values in the AIMD memory function, not reproducible using the Gaussian *Ansatz*. In fact, this is not the case for q values in the 1psBZ. For much larger q very shallow negative minima appear, but they cannot be discarded to be due to numerical noise in the calculation of the second-order memory functions. In any case, this does not appear to be the main problem in the theory regarding the longitudinal dynamics.

As a short note we mention that the weight function for density-density coupling, $\alpha(q,k,p)$, displays a complicated behavior [41] because it is not separable into structural and geometric terms, and it is not straightforward to relate the q variation of $C_L(q,\omega)$ to the changes in $\alpha(q,k,p)$.

V. VELOCITY AUTOCORRELATION FUNCTION

The AIMD calculated $Z(t)$ is shown in Fig. 15 together with the one calculated through the MC approach of Gaskell and Miller [23]. The longitudinal and transverse components of $Z_{\rm GM}(t)$ are also displayed in the figure. We observe that both $Z^L_{\rm GM}(t)$ and $Z^T_{\rm GM}(t)$ show damped oscillations, with the former dominating for larger times because of the smaller damping.

The theory is able to describe very well the simulation results, except in the region near $t = 0$, where we observe some problems related to the limited integration range available.

In the power spectrum $Z(\omega)$, we find two clear peaks, well separated in frequency. The MC results show that the low-frequency peak comes from the contribution of transverse currents, while the high-frequency one corresponds to the longitudinal contribution. Interestingly, the peak frequencies for $Z^T_{\rm GM}(\omega)$ and $Z^L_{\rm GM}(\omega)$ ($\approx$10 and 35 ps^{-1} respectively) are near the values where $C_T(q,\omega)$ and $C_L(q,\omega)$ show maxima for $q \approx q_p/2$. Note that the second maximum of $Z(\omega)$ occurs at somewhat lower frequency that that of $Z^L_{\rm GM}(\omega)$, due to the addition of the tail of the transverse part.

As a final note, the diffusion coefficient obtained from the simulations, $D_{\rm AIMD} = 0.23 \pm 0.01$ Å^2/ps, is very close to the experimental value [44], $D_{\rm exp} = 0.236 \pm 0.006$ Å^2/ps.

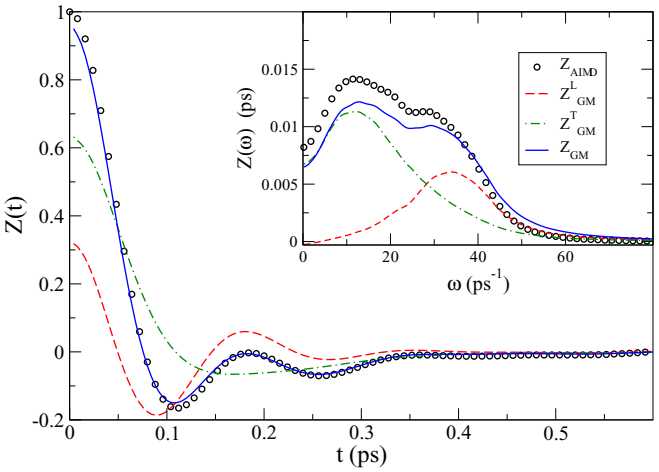

FIG. 15. Normalized velocity autocorrelation function for l-Zn. Symbols denote the AIMD results. The full line is the theoretical MC function, with the dashed and dash-dotted lines representing its longitudinal and transverse components, respectively. The inset shows the corresponding power spectra.

VI. CONCLUSIONS

The present AIMD simulations provide additional support to the experimental suggestion of complex dynamics in liquid Zn, as measured using IXS and INS in the q range within the 1psBZ. Moreover we have shown that this complex dynamics extends to larger q values, above the main peak of $S(q)$, through the appearance of a double mode structure in both the longitudinal and transverse dynamics, a feature previously observed in liquid metals at high pressure and in liquid Ni at room pressure.

Up to now, the origin of such behavior was attributed to couplings between transverse and longitudinal propagation modes, but no theoretical justification had been given. Through the use of mode-coupling concepts we have been able to relate the double mode structure in $C_T(q,\omega)$ to the coupling of the transverse current with density fluctuations at all wave vectors $\vec{k}$, and not only at $\vec{q}$. The analysis of the weight of the different wave vectors in the sum can explain the dispersionless feature of the modes in the range from $q_p/2$ to the first minimum of $S(q)$. Similarly, the double mode structure in $C_L(q,\omega)$ has been traced back to density-density couplings, again including all wave vectors in the integral. However, the theory in its present form is still not able to explain the experimental and computational evidence of an additional mode in $S(q,\omega)$ in the vicinity of $q_p/2$.

We suggest that the inclusion of other coupling modes, particularly the transverse current, will be needed in order to explain the behavior of $S(q,\omega)$ in this region. Such an analysis would help identify if the additional mode can be ascribed a transverse character, or else a different type of character, such as viscoelastic relaxation [45], or heat-wave propagation [46]. It is important from a theoretical point of view to remark again that the mode-coupling formulation takes into account the coupling modes for all wave vectors and not just the one corresponding to the magnitude being studied, so that even if direct coupling is forbidden by symmetry requirements, the mode coupling is still possible. Finally we also suggest that a better treatment of the fast decaying term in the theory may be necessary in order to reproduce quantitatively the structure of the transverse current correlation functions for higher values of q.

The single-particle dynamics, on the other hand, is well described by the mode-coupling theory of Gaskell and Miller. The power spectrum shows two well separated peaks, and this may serve as a hint towards the possible appearance of a double mode structure in the transverse and longitudinal currents, as is indeed the case for l-Zn. Further studies for other systems will be needed in order to support this conjecture.

ACKNOWLEDGMENTS

We acknowledge the financial support of MECD (Grant No. FIS2014-59279-P) jointly with European regional funds. B.G.R. acknowledges the Universidad de Valladolid for the provision of a Ph.D. scholarship.

APPENDIX

We recall that the memory functions are decomposed as the sum of a fast-decaying contribution and a slowly decaying one associated to couplings with slow variables, as specified in Eqs. (9) and (10). The MC theory applied in this work includes couplings with the density mode, which decays slowly not only for $q \to 0$, because of its conserved character, but also in the vicinity of q_p, due to structural correlations. The MC integrals are then written as

$$N^{\mathrm{MC}}(q,t) = \int d\vec{k}\, v_{\rho\rho}(\vec{q},\vec{k},\vec{q}-\vec{k}) \times [F(k,t)F(|\,\vec{q}-\vec{k}\,|,t) - F^f(k,t)F^f(|\,\vec{q}-\vec{k}\,|,t)], \tag{A1}$$

$$M^{\mathrm{MC}}_T(q,t) = \int d\vec{k}\, v_{T\rho}(\vec{q},\vec{k},\vec{q}-\vec{k}) \times [F(k,t)F(|\,\vec{q}-\vec{k}\,|,t) - F^f(k,t)F^f(|\,\vec{q}-\vec{k}\,|,t)], \tag{A2}$$

where $F^f(k,t)$ denotes the fast component of $F(k,t)$, and $v_{\rho\rho}$ and $v_{T\rho}$ are the so-called vertex functions corresponding to the density-density coupling and the transverse current-density coupling respectively. Selecting the z direction as that of $\vec{q}$, their expressions are given by [2]

$$v_{\rho\rho}(\vec{k},\vec{q}-\vec{k}) = \frac{\rho k_B T}{16\pi^3 m}[k_z c(k) + (q-k_z)c(|\,\vec{q}-\vec{k}\,|)]^2, \tag{A3}$$

$$v_{T\rho}(\vec{k},\vec{q}-\vec{k}) = \frac{\rho k_B T}{16\pi^3 m}k_x^2[c(k) - c(|\,\vec{q}-\vec{k}\,|)]^2. \tag{A4}$$

The function $c(q)$ is the direct correlation function, related to the structure factor through the relation $S(q) = [1 - \rho c(q)]^{-1}$. The substraction of the product of the fast components in the integrals has the effect of nullifying the short-time contribution of the integrals to the total function, so that

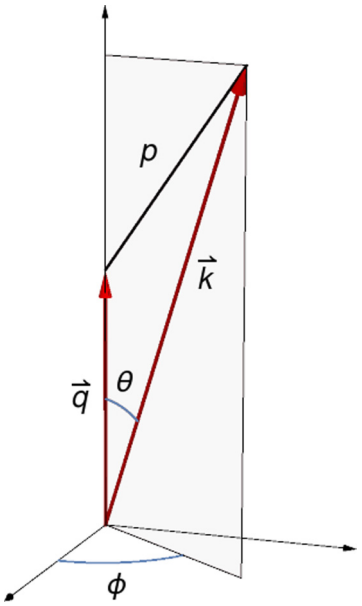

FIG. 16. Two-center bipolar coordinates.

$N^{\mathrm{MC}}(q,t\to 0)\to at^4$, and the same applies to $M_T(q,t\to 0)$. However these terms decay fast and have no influence on the long-time behavior of the functions. In fact the original formulation of MC theories, which focused on the long-time tails, did not include such terms, as we discussed in the text. In any case, the expressions used imply that the short-time characteristics of the memory functions (initial value and first three derivatives) are fully accounted for by the fast contributions. This property is used in the reverse direction, so that an *Ansatz* is formulated for the analytic form of the fast contributions that incorporates the initial value and derivatives of the full memory functions. In this work we use a Gaussian *Ansatz*,

$$N^f(q,t)=N(q,0)\exp\left[-\frac{\mid \ddot{N}(q,0)\mid t^2}{2N(q,0)}\right], \tag{A5}$$

with an equivalent expression for $M_T^f(q,t)$.

For the fast part of $F(q,t)$ we use a different type of *Ansatz*, following Sjögren, given in terms of the single-particle intermediate scattering function $F_s(q,t)$, which we compute from the AIMD simulations, and the free particle expression $F_0(q,t)=\exp[-k_BTq^2t^2/(2m)]$,

$$F^f(q,t)=F(q,t)\frac{F_0(q,t)}{F_s(q,t)}. \tag{A6}$$

Introducing the normalized intermediate scattering function, $F_N(q,t)=F(q,t)/S(q)$, which has an initial value equal to 1 for any q, and the same for its fast part, we finally arrive at mode-coupling integrals in which the time dependence is common to both memory functions, but whose weights for a given $\vec{k}$ vector are different, dictated by the vertex functions, which depend on the structure factor of the liquid and on q, k, and $\mid \vec{q}-\vec{k}\mid$.

Using two-center bipolar coordinates (Fig. 16), so that $p=\mid \vec{q}-\vec{k}\mid$, and performing the ϕ-angular integration explicitly, the final MC integrals read

$$N^{\mathrm{MC}}(q,t)=\frac{\rho k_BT}{8\pi^2m}\frac{1}{q}\int_0^\infty dk\int_{|q-k|}^{q+k}dp\,\alpha(q,k,p)F_N(k,t)F_N(p,t)\left[1-\frac{F_0(k,t)F_0(p,t)}{F_s(k,t)F_s(p,t)}\right], \tag{A7}$$

$$M_T^{\mathrm{MC}}(q,t)=\frac{\rho k_BT}{16\pi^2m}\frac{1}{q}\int_0^\infty dk\int_{|q-k|}^{q+k}dp\,\gamma(q,k,p)F_N(k,t)F_N(p,t)\left[1-\frac{F_0(k,t)F_0(p,t)}{F_s(k,t)F_s(p,t)}\right], \tag{A8}$$

where

$$\alpha(q,k,p)=kS(k)pS(p)\left[\frac{q^2+p^2-k^2}{2q}\left(\frac{S(k)-1}{S(k)}\right)+\frac{q^2+k^2-p^2}{2q}\left(\frac{S(p)-1}{S(p)}\right)\right]^2 \tag{A9}$$

and

$$\gamma(q,k,p)=-\frac{kp[S(k)-S(p)]^2}{S(k)S(p)}\frac{(q-k-p)(q-k+p)(q+k-p)(q+k+p)}{4q^2}. \tag{A10}$$

Note that the integration region for a given q is a strip in the (k,p) plane, symmetric with respect to its diagonal, $p=k$, whose width depends on q. Moreover, both $\alpha(q,k,p)$ and $\gamma(q,k,p)$ are symmetric with respect to interchanging k and p, i.e., both functions are symmetric with respect to the diagonal.

These functions quantify the degree of coupling between the functions at wave vector $\vec{q}$ and at given values of k and p, i.e., at wave vector $\vec{k}$, and both are non-negative (the product of the latter four terms in $\gamma(q,k,p)$ is always negative or zero in the integration strip). The function $\gamma(q,k,p)$ factorizes into a structural term and a "geometric" term purely dependent on the wave numbers. The geometric factor is zero at the borders of the strip, and the structural term is zero at the diagonal, so $\gamma(q,k,p)$ takes null values in several parts of the integration region, somehow reflecting the "difficulty" for transverse-longitudinal coupling. On the contrary, $\alpha(q,k,p)$ only becomes zero for particular (k,p) pairs that nullify the term inside brackets, for instance in the diagonal $p=k$ at k values where $S(k)=1$. This basically reflects that longitudinal-longitudinal couplings are much easier than transverse-longitudinal ones.

Once the fast terms [Eq. (A5)] and MC terms [Eqs. (A7) and (A8)] have been evaluated, the full memory functions are obtained and, from these, using the memory function equation

in Laplace space and the relation between FT and LT, we obtain

$$C_T(q,\omega) = \frac{k_B T}{\pi m}\mathrm{Re}\left[\frac{1}{i\omega + \tilde{M}_T(q,i\omega)}\right], \qquad \text{(A11)}$$

where Re denotes the real part. Since the LT is a complex magnitude we write $\tilde{M}_T(q,i\omega) = M_{T,c}(q,\omega) - iM_{T,s}(q,\omega)$, where the labels c and s denote integration of the function multiplied by $\cos(\omega t)$ and $\sin(\omega t)$ respectively. After taking the real part we get

$$C_T(q,\omega) = \frac{k_B T}{\pi m}\frac{M_{T,c}(q,\omega)}{M^2_{T,c}(q,\omega) + \left[\omega - M_{T,s}(q,\omega)\right]^2}. \qquad \text{(A12)}$$

Following exactly the same approach for $N(q,t)$, we can directly obtain $S(q,\omega)$ and $C_L(q,\omega)$ from $N_c(q,\omega)$ and $N_s(q,\omega)$.

[1] J. P. Hansen and I. R. McDonald, *Theory of Simple Liquids* (Academic, London, 1986).

[2] U. Balucani and M. Zoppi, *Dynamics of the Liquid State* (Clarendon, Oxford, 1994).

[3] S. Hosokawa, M. Inui, Y. Kajihara, K. Matsuda, T. Ichitsubo, W.-C. Pilgrim, H. Sinn, L. E. González, D. J. González, S. Tsutsui, and A. Q. R. Baron, Phys. Rev. Lett. **102**, 105502 (2009).

[4] V. M. Giordano and G. Monaco, Proc. Natl. Acad. Sci. USA **107**, 21985 (2010); Phys. Rev. B **84**, 052201 (2011).

[5] S. Munejiri, F. Shimojo, and K. Hoshino, Phys. Rev. B **86**, 104202 (2012); S. Hosokawa, S. Munejiri, M. Inui, Y. Kajihara, W.-C. Pilgrim, Y. Ohmasa, S. Tsutsui, A. Q. R. Baron, F. Shimojo, and K. Hoshino, J. Phys.: Condens. Matter **25**, 112101 (2013).

[6] S. Hosokawa, M. Inui, Y. Kajihara, S. Tsutsui, and A. Q. R. Baron, J. Phys.: Condens. Matter **27**, 194104 (2015).

[7] M. Zanatta, F. Sacchetti, E. Guarini, A. Orecchini, A. Paciaroni, L. Sani, and C. Petrillo, Phys. Rev. Lett. **114**, 187801 (2015).

[8] M. Marqués, L. E. González, and D. J. González, Phys. Rev. B **92**, 134203 (2015).

[9] M. Marqués, L. E. González, and D. J. González, J. Phys.: Condens. Matter **28**, 075101 (2016).

[10] M. Marqués, D. J. González, and L. E. González, Phys. Rev. B **94**, 024204 (2016).

[11] B. G. del Rio, L. E. González, and D. J. González, J. Chem. Phys. **146**, 034501 (2017).

[12] T. Bryk, G. Ruocco, T. Scopigno, and A. P. Seitsonen, J. Chem. Phys. **143**, 104502 (2015).

[13] W. Götze, Condens. Matter Phys. **1**, 873 (1998).

[14] R. Zwanzig, in *Boulder Lectures in Theoretical Physics*, edited by W. E. Brittin, B. W. Downs, and J. Downs (Wiley Interscience, New York, 1961), Vol. III, p. 106; H. Mori, Prog. Theor. Phys. **33**, 423 (1965).

[15] A. Aguado, A. Vega, A. Lebon, and B. von Issendorff, Angew. Chem. **54**, 2111 (2015).

[16] W. B. Pearson, *Handbook of Lattice Spacings and Structures of Metals and Alloys* (Pergamon, Oxford, 1958).

[17] Y. Waseda, *The Structure of Non-Crystalline Materials* (McGraw-Hill, New York, 1980); http://res.tagen.tohoku.ac.jp/~waseda/scm/LIQ/all/zn.html

[18] D. M. North, J. E. Enderby, and P. A. Egelstaff, J. Phys. C **1**, 1075 (1968).

[19] H. Lou, X. Wang, Q. Cao, D. Zhang, J. Zhang, T. Hu, H.-k. Mao, and J.-Z. Jiang, Proc. Natl. Acad. Sci. USA **110**, 10068 (2013).

[20] P. Hohenberg and W. Kohn, Phys. Rev. **136**, B864 (1964); W. Kohn and L. J. Sham, *ibid.* **140**, A1133 (1965).

[21] L. Sjögren and A. Sjölander, J. Phys. C **12**, 4369 (1979).

[22] G. Wahnström and L. Sjögren, J. Phys. C **15**, 401 (1982).

[23] T. Gaskell and S. Miller, J. Phys. C **11**, 3749 (1978); Phys. Lett. A **66**, 307 (1978).

[24] A. Delisle, D. J. González, and M. J. Stott, Phys. Rev. B **73**, 064202 (2006).

[25] G. Kresse and J. Hafner, Phys. Rev. B **47**, 558 (1993); **49**, 14251 (1994); G. Kresse and J. Furthmuller, *ibid.* **54**, 11169 (1996); Comput. Mater. Sci. **6**, 15 (1996).

[26] U. Bafile, E. Guarini, and F. Barocchi, Phys. Rev. E **73**, 061203 (2006).

[27] J.-F. Wax and T. Bryk, J. Phys.: Condens. Matter **25**, 325104 (2013); S. Bellissima, M. Neumann, E. Guarini, U. Bafile, and F. Barocchi, Phys. Rev. E **92**, 042166 (2015).

[28] M. H. Ernst, E. H. Hauge, and J. M. J. van Leeuwen, Phys. Rev. Lett. **25**, 1254 (1970); Phys. Rev. A **4**, 2055 (1971); J. Stat. Phys. **15**, 7 (1976).

[29] I. M. de Schepper and M. H. Ernst, Physica **98A**, 189 (1979)

[30] M. H. Ernst and J. R. Dorfman, Physica **61**, 157 (1972); J. Stat. Phys. **12**, 311 (1974).

[31] W. Schirmacher and H. Sinn, Condens. Matter Phys. **11**, 127 (2008).

[32] L. Sjögren, Phys. Rev. A **22**, 2866 (1980).

[33] D. Levesque and L. Verlet, Phys. Rev. A **2**, 2514 (1970).

[34] L. Sjögren, J. Phys. C **13**, 705 (1980); Phys. Rev. A **22**, 2883 (1980).

[35] U. Balucani, R. Vallauri, T. Gaskell, and S. F. Duffy, J. Phys.: Condens. Matter **2**, 5015 (1990); U. Balucani, A. Torcini, and R. Vallauri, Phys. Rev. A **46**, 2159 (1992); J. Non-Cryst. Solids **156-158**, 43 (1993); Phys. Rev. B **47**, 3011 (1993); U. Balucani, A. Torcini, A. Stangle, and C. Morkel, Phys. Scr. **T57**, 13 (1995).

[36] W. Gudowski, M. Dzugutov, and K.-E. Larsson, Phys. Rev. E **47**, 1693 (1993).

[37] F. Shimojo, K. Hoshino, and M. Watabe, J. Phys. Soc. Jpn. **63**, 1821 (1994); K. Hoshino, F. Shimojo, and S. Munejiri, *ibid.* **71**, 119 (2002).

[38] L. E. González, D. J. González, and M. Canales, Z. Phys. B **100**, 601 (1996); J. Casas, D. J. González, and L. E. González, Phys. Rev. B **60**, 10094 (1999); J. Casas, D. J. González, L. E. González, M. M. G. Alemany, and L. J. Gallego, *ibid.* **62**, 12095 (2000); L. E. González, D. J. González, and J. Casas, J. Non-Cryst. Solids **312-314**, 158 (2002).

[39] M. Canales and J. A. Padró, J. Phys.: Condens. Matter **9**, 11009 (1997); Phys. Rev. E **63**, 011207 (2000).

[40] B. Schmid and W. Schirmacher, J. Phys.: Condens. Matter **23**, 254211 (2011).

[41] See Supplemental Material at http://link.aps.org/supplemental/10.1103/PhysRevB.95.224201 for details about the numerical integration procedure and the structure of the weight function $\alpha(q,k,p)$.

[42] M. Ranganathan and H. C. Andersen, J. Chem. Phys. **121**, 1243 (2004).

[43] M. Ranganathan and H. C. Andersen, J. Phys. Chem. B **109**, 21437 (2005).

[44] N. H. Nachtrieb, E. Fraga, and C. Wahl, J. Phys. Chem. **67**, 2353 (1963).

[45] E. Guarini, U. Bafile, F. Barocchi, A. De Francesco, E. Farhi, F. Formisano, A. Laloni, A. Orecchini, A. Polidori, M. Puglini, and F. Sacchetti, Phys. Rev. B **88**, 104201 (2013).

[46] T. Bryk and J.-F. Wax, J. Chem. Phys. **144**, 194501 (2016).